Solar Energetic Particle Events of July 2017: Multi-spacecraft Observations near 1 and 1.5 AU

C. Krishnaprasad[1,2], Smitha V. Thampi[1], Christina O. Lee[3], Srikar P. Tadepalli[4], K. Sankarasubramanian[4], and Tarun K. Pant[1]

[1]Space Physics Laboratory, Vikram Sarabhai Space Centre, Thiruvananthapuram 695022, India
[2]Cochin University of Science and Technology, Kochi 682022, India
[3]Space Sciences Laboratory, University of California, Berkeley, CA 94720, USA
[4]U. R. Rao Satellite Centre, Bengaluru 560017, India

Key Points:

- Multi-spacecraft observations of the solar events of late solar cycle 24 in July 2017 are presented. Observations near Earth, STEREO-A, and near Mars are used.
- Solar Energetic Particle (SEP) proton enhancement is observed at a remote observer location due to IMF connectivity with a distant CME-driven shock.
- Spectral analysis of the SEP events associated with CMEs and SIRs are carried out and the spectral features are interpreted in terms of acceleration, transport, and magnetic connectivity.

Corresponding author: C. Krishnaprasad, kpchirakkil@gmail.com

Abstract

We investigate the solar events of late solar cycle 24 in July 2017 observed by a number of spacecraft in the inner heliosphere widely separated in heliolongitude and radial distance. These include spacecraft at L1 point, STEREO-A, near Earth satellites, and MAVEN (near Mars). The GRASP payload onboard Indian GSAT-19 satellite provides a new vantage point for Solar Energetic Particle (SEP) observations near Earth. There were two major Coronal Mass Ejections (CMEs) and a Stream Interaction Region (SIR) event in July 2017, which is a period during the deep descending phase of the historically weak solar cycle 24. The 16 July CME was Earth directed and the 24 July CME was STEREO-A and Mars directed. Earth and Mars were on the opposite sides of the solar disk, while Mars and STEREO-A were aligned with respect to the nominal Parker spiral field. The 24 July event was stronger and wider in heliolongitude. This CME-driven shock had magnetic connectivity to Earth, which produced an SEP event at Earth ∼two days later. The spectral indices of the event observed directly at STEREO-A and at the remote location of ACE was found to be similar. The 16 July SIR event was observed by both MAVEN and STEREO-A. Higher particle intensities (a factor of 6 enhancement for 1 MeV protons) are observed by MAVEN (at 1.58 AU) compared to STEREO-A (at 0.96 AU). Also a spectral hardening is observed while comparing the spectral indices at these two locations, indicating proton acceleration at the SIR forward shock during the radial propagation of 0.62 AU in the interplanetary space.

1 Introduction

Solar Energetic Particles (SEPs) are the high energy protons, electrons, alpha particles, and heavy ions released from the Sun and accelerated at or near the Sun or in the heliosphere (e.g. recent reviews by Desai and Giacalone (2016); Klein and Dalla (2017)). These particles are of energies in the range tens of keV upto a few GeV. Solar flares, Coronal Mass Ejections (CMEs), and Stream Interaction Regions (SIRs) are major sources of energetic particles in the inner heliosphere. Interplanetary acceleration by SIR and interplanetary shocks can further act on SEPs to modify their properties. CMEs are ejection of plasma and magnetic field from the solar corona, typically remote-sensed by coronagraphs. SIRs are interaction regions formed in the heliosphere when the high velocity portion of a trailing stream overtakes the low velocity region of the preceding stream (Smith & Wolfe, 1976), and corotating interaction regions (CIRs) are solar wind stream structures that persists over several solar rotations, leading to repeated occurrence of stream interactions such that they co-rotate with the Sun (Balogh, Gosling, Jokipii, Kallenbach, & Kunow, 1999; Richardson, 2018). These transient solar events have severe impacts on the atmosphere and ionosphere of Earth (e.g. B. T. Tsurutani et al. (2009)) as well as on unmagnetized planets, such as increased atmospheric loss at Mars (e.g. Krishnaprasad, Thampi, and Bhardwaj (2019); Lee et al. (2018); Thampi et al. (2018)).

The SEPs undergo changes in their properties, such as they accelerate at flare sites or at interplanetary shocks upon traveling through the heliosphere (Pesses, Van Allen, Tsurutani, & Smith, 1984; B. T. Tsurutani, Smith, Pyle, & Simpson, 1982). It is also observed that the energetic particle increases in intensity–time profiles have well–defined forms dependent on the location of the source relative to the observer and the presence and strength of interplanetary shocks and shock normal angle (Cane, Reames, & von Rosenvinge, 1988; Reames, 1995; B. T. Tsurutani & Lin, 1985; Van Hollebeke, Ma Sung, & McDonald, 1975). The SEP events are broadly classified into ‘gradual’ and ‘impulsive’ based on the intensity rise rate and duration, and particle compositions (Reames, 1995, 2013). Gradual SEP events are dominated by high-energy protons (that is, large p/e ratios) with normal ion abundance ratios and charge states, while impulsive SEP events are dominated by 0.1-100 keV electrons (that is, small p/e ratios) with enhanced ^{3}He (and heavier ion) emissions and charge states.

Parker (1958) suggested that interplanetary magnetic field (IMF) lines form an Archimedean spiral in the solar equatorial plane, assuming the footpoints of the magnetic field lines are fixed in the photosphere, which rotates with the Sun. An enhancement in SEP flux is observed at a vantage point either when the shock associated with a stream or ejection directly passes the observer, or if the IMF is connected to the observer site (as the charged particles can gyrate and move along the field lines, i.e. parallel transport from the source to the observer), or because of perpendicular transport by cross–field diffusion or drift (Zhang, Qin, & Rassoul, 2009). The particles are generally accelerated in CME-driven shocks close to the Sun (∼3–10 solar radii, i.e. within 1 AU), as well as beyond and are streamed out through the heliosphere following magnetic field lines (Chollet et al., 2010). These gradual events are observed over a wide longitude interval, unlike the impulsive events which are restricted to $< 30°$ longitude cone (Reames, 1995). The intensity peak near the shock is generally called the energetic storm particle event. In large CME-related SEP events, changes in field line connectivity of the spacecraft to different particle acceleration regions will result in changes in intensity–time profiles.

Recently, Xie, Mkel, St.Cyr, and Gopalswamy (2017) studied three SEP events observed in the solar cycle 23 by STEREO A, B, and near-Earth (L1) spacecraft with a wide longitudinal distribution of particles. They examined whether the observations of SEPs from different vantage points could be explained by acceleration and injection by the spatially extended shocks or whether another mechanism such as cross-field transport is required, and found that cross-field diffusion is the likely candidate for some of the enhancements observed with wide longitudinal spread. Cross-field diffusion can result from interactions between energetic protons and magnetic field magnitude decreases (da Costa Jr., Tsurutani, Alves, Echer, & Lakhina, 2013; B. T. Tsurutani & Thorne, 1982). The magnetically connected SEP intensities are often found to be an order of magnitude lower than the SEPs directly coming to the observer location (Xie et al., 2017). Simultaneous observations of SEP events using a constellation of spacecraft, at different longitudes and radial positions, may give us an idea of how the longitudinal spread of the SEP intensity varies, in addition to other observables.

The SEP events of July 2017 are special in a sense that these are quite intense and appeared in the deep descending-to-minimum phase of the historically weak solar cycle 24 (Liu, Zhao, Hu, Vourlidas, & Zhu, 2019; Luhmann et al., 2018; Paouris & Mavromichalaki, 2017). This is surprising, as we do not expect such intense energetic particle events in the declining and late phase of a solar cycle (during solar maximum, there are typically mainly CMEs, whereas in the period of study during the decay phase, there are both CMEs and SIRs). But such exceptional solar activity is not unprecedented and in fact the late solar cycle 23 also had such SEP events (von Rosenvinge et al., 2009). There are a few studies on the CMEs and associated energetic particle events of July 2017, and their space weather impacts. The energetic particles associated with the 16 July 2017 Earth directed CME event arrived with a delay at the Magnetospheric Multiscale Mission due to the magnetic connectivity of the satellite (Blake, Fennell, Turner, Cohen, & Mauk, 2019). There was a prompt enhancement in Earth's radiation belt electron flux during the CME-shock compression and subsequent geomagnetic storm, observed by the Relativistic Electron Proton Telescope instrument on board Van Allen Probes (Patel, Li, Hudson, Claudepierre, & Wygant, 2019). They used an MHD-test particle simulation to reproduce the observations. During the 24 July 2017 CME event, a multistep Forbush decrease with a remarkable total amplitude of more than 15% was observed by Mars Science Laboratory/Radiation Assessment Detector at Mars (Dumbović et al., 2019).

The combination of observations performed simultaneously by several spacecrafts located at various heliospheric locations is a tool to investigate the spatial distribution of SEP events. Using measurements from widely separated spacecrafts in longitude and radial distance in the inner heliosphere, we examine SEP proton intensity–time profiles present in the July 2017 events and discuss their attributes in the context of the Sun, state of the surrounding heliosphere, in situ plasma and magnetic field signatures, spacecraft's magnetic connectivity to the shock, and the spectral differences at these locations.

2 Data and Method

The solar disk images are from the Solar Dynamics Observatory (SDO) Atmospheric Imaging Assembly (AIA; `https://sdo.gsfc.nasa.gov/`) and Solar TErrestrial RElations Observatory Ahead (STEREO-A) Sun Earth Connection Coronal and Heliospheric Investigation (SECCHI) Extreme Ultraviolet Imager (EUVI; `https://stereo-ssc.nascom.nasa.gov/`). The white-light coronagraph images are from the Solar and Heliospheric Observatory (SOHO) Large Angle and Spectrometric Coronagraph (LASCO)-C2 and STEREO-A/SECCHI Coronagraph-2 (COR2).

The energetic proton observations from the first Sun–Earth Lagrange point (L1 at ∼0.99 AU) are from the Low Energy Magnetic Spectrometer (LEMS) of Electron Proton Alpha Monitor (EPAM) sensor onboard the Advanced Composition Explorer (ACE) spacecraft (Gold et al., 1998). The ACE Solar Wind Electron Proton Alpha Monitor (SWEPAM) and magnetic field experiment (MAG) measurements are used for IMF and solar wind speed observations at 1 AU. The observations near Earth are from the Energetic Particle Sensor (EPS) onboard Geostationary Operational Environmental Satellites (GOES-13), Geostationary Radiation Spectrometer (GRASP) onboard Geostationary Satellite (GSAT-19), and the Solid State Telescope (SST) onboard Acceleration Reconnection Turbulence and Electrodynamics of the Moon's Interaction with the Sun (ARTEMIS) spacecraft. The STEREO-A Solar Electron Proton Telescope (SEPT; Müller-Mellin et al. (2008)), Low Energy Telescope (LET; Mewaldt et al. (2008)), and High Energy Telescope (HET; Richardson et al. (2014); von Rosenvinge et al. (2008)) particle telescopes are also used for energetic proton observations at 1 AU from a different heliospheric longitude with respect to near–Earth spacecraft. The In-situ Measurements of Particles and CME Transients (IMPACT)/Magnetometer (MAG) magnetic field and PLAsma and SupraThermal Ion Composition (PLASTIC) solar wind plasma measurements are used for IMF and solar wind observations from STEREO-A. The GOES-13 differential and integral fluxes are taken from OMNIWeb data center (`https://omniweb.gsfc.nasa.gov/`). The ACE data are obtained from ACE Science Center (`http://www.srl.caltech.edu/ACE/ASC/`) and the STEREO-A data are obtained from STEREO Science Center (`http://www.srl.caltech.edu/STEREO/`). The ARTEMIS data are obtained from `http://artemis.ssl.berkeley.edu/`.

GSAT-19 is an Indian communication satellite launched in June 2017 that carries GRASP payload to monitor and study the nature of charged particles and the influence of space radiation on satellites and their electronic components. The instrument measures the energy and flux of incident particles, and also enables particle identification by the E–dE technique. GSAT-19 is orbiting in 82°E longitude, while GOES-13 was at 75°W longitude of Earth. The in situ measurements from GRASP can provide additional data from geostationary orbit that can lead to improved models on space radiation.

The Solar Energetic Particle (SEP) instrument onboard Mars Atmosphere and Volatile EvolutioN (MAVEN) spacecraft in orbit around Mars provides SEP proton and electron observations near 1.5 AU (Larson et al., 2015). This instrument consists of two identical sensors, SEP 1 and SEP 2, each consisting of a pair of double-ended solid-state telescopes to measure 20 keV–200 keV electrons and 20 keV–6 MeV protons in four orthogonal view directions that are positioned to adequately cover the canonical Parker spiral direction around which SEP distributions are centered (Larson et al., 2015). The data used in this study are the proton data in the form of energy fluxes measured by the SEP 1 sensor in the forward and reverse looking fields of view (FOV). The proton counts measured by SEP/MAVEN in the lower energy channels ($<$ 100 keV) are also contributed by the O^+ pickup ions from Mars, and hence are removed from the analysis (Larson et al., 2015; Rahmati et al., 2015). The upstream solar wind velocity from Solar Wind Ion Analyzer

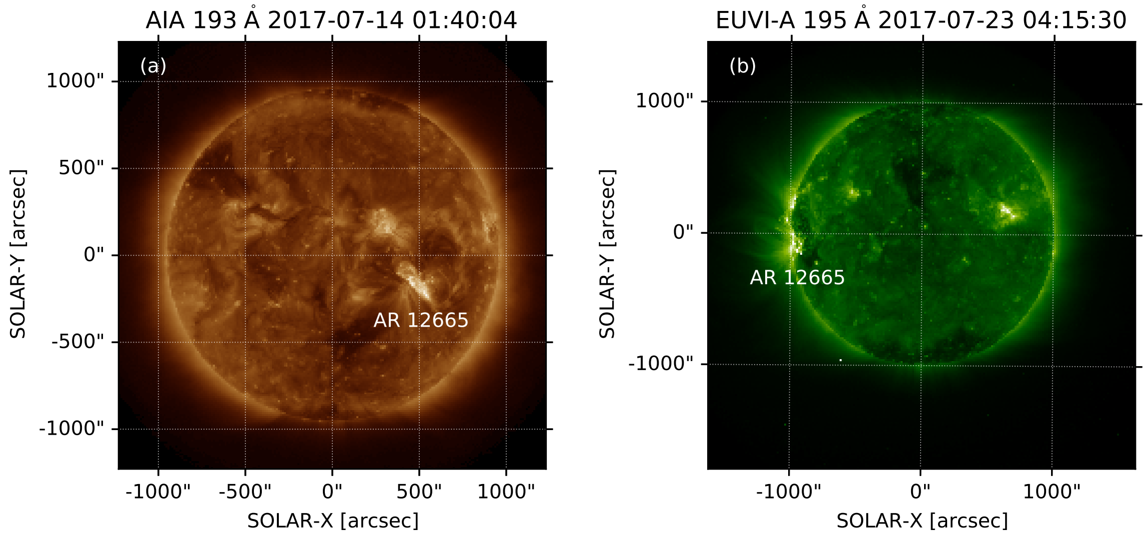

Figure 1. CME eruption site near AR 12665 on the solar disk imaged by (a) SDO/AIA on 14 July, 01:40 UT and (b) STEREO-A/EUVI on 23 July, 04:15 UT.

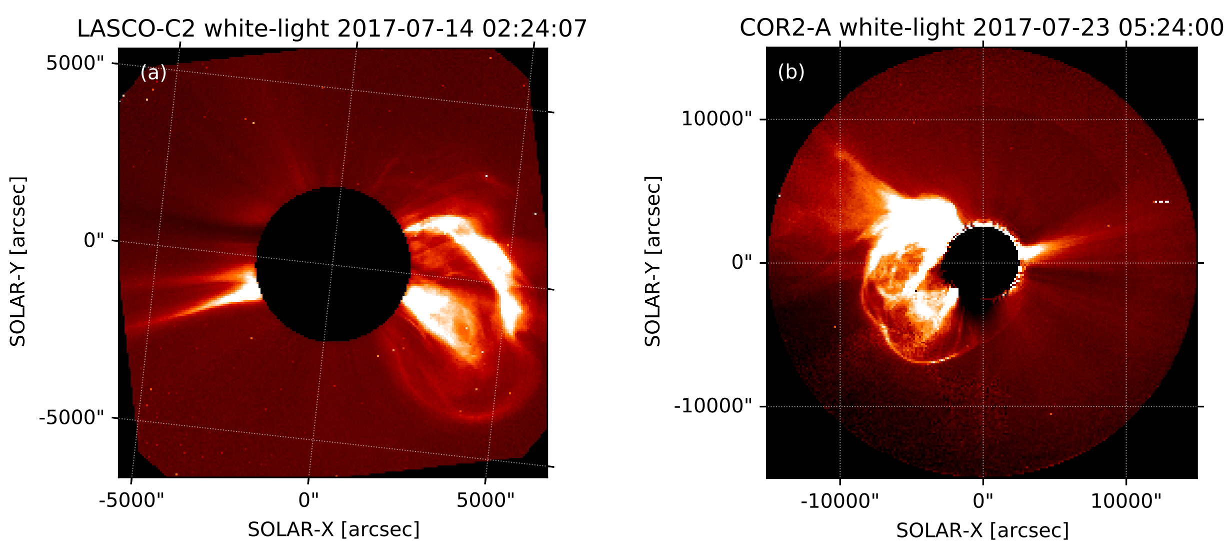

Figure 2. (a) CME1 structure on 14 July, 02:24 UT by SOHO/LASCO C2 and (b) CME2 structure on 23 July, 05:24 UT by STEREO-A/COR2.

(SWIA) and IMF from Magnetometer (MAG) are obtained using the method given by Halekas et al. (2017). The method is based on the measured solar wind bulk flow speed ($|v|$), proton scalar temperature (T), altitude (R), and normalized magnetic field fluctuation levels ($\sigma_B/|B|$). Here, σ_B is the root-sum-squared value of the 32 Hz fluctuation levels in all three magnetic field components over a 4 sec interval and $|B|$ is the total magnetic field. To select undisturbed solar wind intervals (in each orbit), points with $|v| > 200$ km/s, $\sigma_B/|B| < 0.15$, R $>$ 500 km, and $\sqrt{T}/|v| < 0.012$ are chosen (Halekas et al., 2017). The MAVEN data are obtained from the Planetary Data System (`https://pds.nasa.gov/`).

During July 2017, both STEREO-A and Mars were located at the back side of the Sun as viewed from Earth. STEREO-A was at -132° HEE (Heliocentric Earth Ecliptic) longitude, and Mars was at $\sim$ -178° HEE longitude, with a longitudinal separation of $\sim$46° between STEREO-A and Mars (with Earth being at a reference heliolongitude of 0°). Mars was at a radial distance of 1.58 AU from the Sun, while STEREO-A was at $\sim$0.96 AU during this period.

The Wang-Sheeley-Arge (WSA)-ENLIL+Cone model simulations (Mays et al., 2015; Odstrcil, 2003) are taken from Community Coordinated Modeling Center (CCMC; `https://ccmc.gsfc.nasa.gov/`). This combined time-dependent model consists of solar coronal model WSA coupled with the global heliospheric solar wind magnetohydrodynamic (MHD) model ENLIL, and CMEs (spherical shaped high pressure gusts) inserted using Cone model–3D CME kinematic and geometric parameters. The inputs to the model simulations shown in Figures 1 and 2 (such as the National Solar Observatory (NSO) Global Oscillation Network Group (GONG) Potential Field Source Surface (PFSS) synoptic magnetic field maps and Cone model parameters) are described in Luhmann et al. (2018). The simulations gives a global heliospheric context during the events, as well as the relative planetary and spacecraft positions. The simulated solar wind velocities appear to capture the ACE and STEREO-A observed velocities, thus giving confidence on the wider inner heliospheric simulations (Luhmann et al., 2018).

3 Observations

There were two major CME eruptions during July 2017. The NOAA Active Region (AR) 12665 (located around source coordinate S07W44 (652", -165")) was the prominent eruptive region on the Sun during this period (Luhmann et al., 2018). The SDO Helioseismic and Magnetic Imager (HMI) showed the presence of a dark sunspot associated with AR 12665. The main eruptions for the period were multiple, with fast and wide ejections following one another by roughly a week with the CME ejecta headed first to the west of Earth and then later in the general direction of STEREO-A and Mars (Luhmann et al., 2018). Figure 1a shows the SDO/AIA image of the solar disk at 193 Å, and Figure 1b shows the STEREO-A EUVI image of the solar disk at 195 Å. Both images indicate the presence of eruption site near the active region, as well as the presence of CME loops.

Figure 2 shows the CME structures observed by the white-light coronagraphs onboard SOHO and STEREO-A during the two major interplanetary CME events of July. The SOHO/LASCO C2 coronagraph image (Figure 2a) and STEREO-A/COR2 coronagraph image (Figure 2b) show the CME eruptions. The CME on 14 July (hereafter CME1) first appeared in LASCO-C2 at 01:25 UT and in LASCO-C3 at 02:18 UT, which is consistent with their FOV and an initial CME linear speed of $\sim$1200 km sec^{-1} (`https://cdaw.gsfc.nasa.gov/CME_list/`). The CME on 23 July (hereafter CME2) first appeared in STEREO-A COR-2 at 04:54 UT (`http://spaceweather.gmu.edu/seeds/secchi.php`). The CME1 had an associated C-class flare and a long-duration ($\sim$116 min.) M2.4-class flare originated from AR 12665, while the CME2 had two associated B-class flares originated from the same active region (Dumbović et al., 2019).

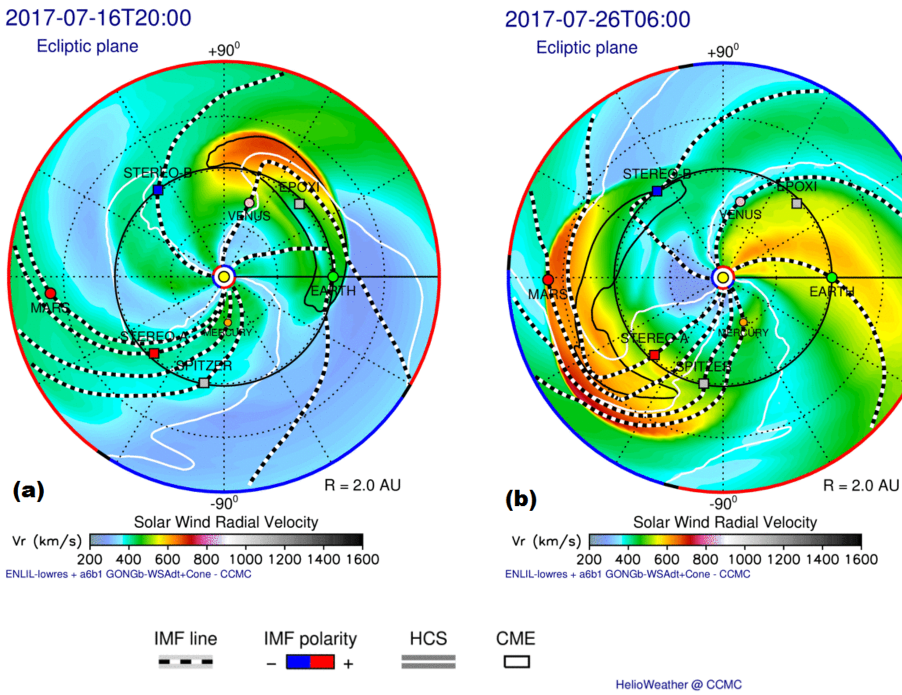

Figure 3. The snapshots of WSA-ENLIL+Cone model simulations of inner heliospheric conditions such as solar wind radial velocity (color contour) and IMF lines (black and white lines) during (a) 14 to 20 July 2017 event at Earth (CME1 event) and (b) 23 to 28 July 2017 event at STEREO-A and Mars (CME2 event).

Figure 3 shows the snapshots of WSA-ENLIL+Cone model (hereafter ENLIL) simulations of inner heliospheric conditions such as solar wind radial velocity and IMF lines during 14 to 20 July 2017 event at Earth (CME1; Figure 3a) and 23 to 28 July 2017 event at STEREO-A and Mars (CME2; Figure 3b). The event period ENLIL simulation results for July are described in detail by Luhmann et al. (2018). The July 2017 events seemed to arise in conjunction with the appearance of a coronal pseudostreamer (Luhmann et al., 2018). The simulations show the magnetic field lines during the event period, and some of which connects between the spacecraft and the CME from inside as well as from outside the spacecraft heliocentric radius. Luhmann et al. (2018) calculated the shock connection radius, which shows that Earth is connected to shocks from outside 1 AU during the CME2 event.

Figure 4 shows the solar wind proton velocity, temperature, and magnetic field observations by ACE and STEREO-A, during the two CME events and a SIR event in July 2017. The shock arrival is identified based on the discontinuities/jumps in the plasma and field observations. The shocks in the STEREO-A plasma and magnetic field data are identified in the STEREO-A interplanetary shock list (`https://stereo-ssc.nascom.nasa.gov/data/ins_data/impact/level3/STEREO_Level3_Shock.pdf`). The forward and reverse shocks in STEREO Level 3 shocks list are identified using 8 sec^{-1} magnetic field data, which is rotated into shock normal coordinates to examine the existence of associated shock waves and field changes consistent with the Rankine-Hugoniot relations (Jian et al., 2013; B. Tsurutani et al., 2011). At forward shocks, solar wind speed, proton temperature, and magnetic field increase simultaneously, whereas at reverse shocks, solar wind speed increases, while proton temperature, and magnetic field decrease (Jian et al., 2013). Shocks and their sheaths are not part of CMEs, and CME shocks only exist for fast CMEs and first form when the speed

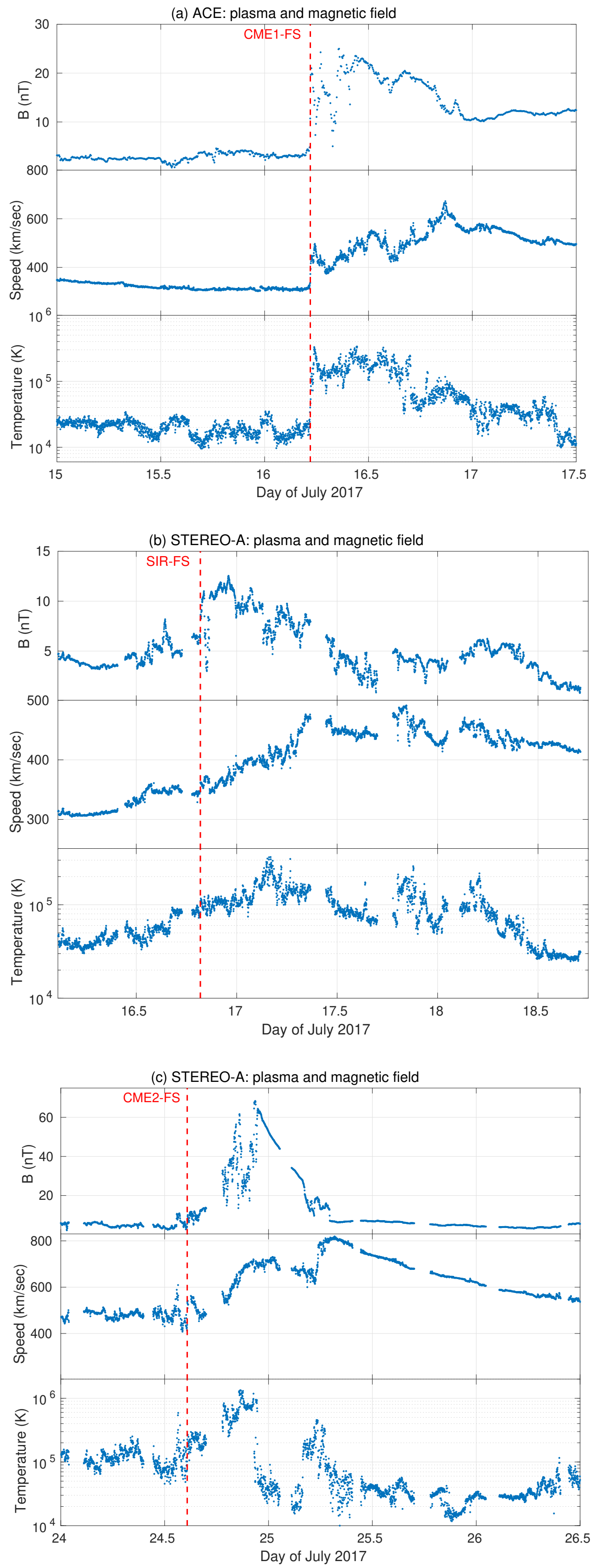

Figure 4. (a) The 16 July CME1-shock arrival observed by ACE, (b) The 16 July SIR-shock arrival observed by STEREO-A, and (c) The 24 July CME2-shock arrival observed by STEREO-A.

of the CME is faster than the local magnetosonic speed (Tsurutani, B., Wu, S. T., Zhang, T. X., & Dryer, M., 2003). This occurs somewhere between 5 and 10 solar radii depending on the local plasma conditions. Slow (submagnetosonic) CMEs do not form shocks and therefore do not accelerate energetic particles (B. Tsurutani, Gonzalez, Zhou, Lepping, & Bothmer, 2004). Although not all shocks have clear signatures in plasma properties, the two fast CME events and the SIR event described here has clear plasma and magnetic field signatures of forward shock (FS) arrivals (Figure 4). The CME1 shock arrives at L1 on 16 July, 05:16 UT (Figure 4a), SIR shock arrives at STEREO-A on 16 July, 19:39 UT (Figure 4b), and CME2 shock arrives at STEREO-A on 24 July, 14:36 UT (Figure 4c). The shock arrivals at Mars location is not shown since we do not have high time resolution and continuous upstream solar wind and IMF data from the MAVEN spacecraft (as the orbit of MAVEN is elliptical with nominal periapsis around 150-160 km, and the spacecraft watching the "pure" solar wind only during a segment of the orbit as described earlier).

The CME1 event observed at L1 point by ACE spacecraft and at Earth's geostationary orbit by GOES and GSAT-19 satellites was due to an Earth directed CME. Figure 5a shows the IMF and solar wind velocity observed by ACE during 12 to 31 July 2017. A fluctuating IMF with increase in total $|B|$ to $\sim$25 nT and an increase in solar wind speed to 664 km sec^{-1} was observed. Figure 5b shows the SEP intensity–time profiles of energetic protons in different energy channels (between $\sim$100 keV and 4.75 MeV) observed by EPAM/ACE. The energetic proton intensities increase gradually from 14 July upto 20 July, with a crescendo observed on 16 July. The peak flux during this period in the lowest energy channel (110 keV to 190 keV) was 3×10^5 pfu MeV^{-1} (here the particle flux unit, 1 pfu = 1 particle cm^{-2} s^{-1} sr^{-1}). The sudden spikes in the intensity profiles, such as those seen on 22 July are due to the accelerated ions propagating from the Earth's bow shock (Bruno, Christian, de Nolfo, Richardson, & Ryan, 2019). The event was also observed by GOES and GSAT-19. The proton flux enhancement can be seen from 14 to 16 July with a peak enhancement of 12 pfu in GOES >10 MeV channel and 7 pfu in GSAT-19/GRASP 5-85 MeV channel (Figure 5c). The GRASP data are being used for the first time, and therefore the comparison of GRASP with GOES also serves as a validation for GRASP observations. The enhancement seen at GOES and GSAT is before the peak flux observed at ACE. This is because the GOES and GSAT detected protons are of higher energies, which travel faster than the comparatively low-energy SEPs observed by ACE. The combination of ACE (lower energy) and GOES/GRASP (higher energy) shows population evolution by velocity dispersion, where the most energetic protons arrive first, $\sim$a day before the CME plasma and field disturbance. This event was also observed by the solid state telescopes onboard ARTEMIS P1 and P2 (the former THEMIS b and c satellites) in orbit around Moon. The observed intensity–time profiles of 100 keV to 6 MeV energetic protons are similar to the ACE observations (not illustrated). Hence, the observations from ACE and ARTEMIS provide independent measurements of the same events at similar energies, and it is important to note that these particles are observed near the Lunar orbit as well. The CME1 event caused a geomagnetic storm with disturbance storm time index, Dst$_{min}$ of -72 nT observed on 16 July $\sim$15 UT.

The CME2 (second major event of July), starting from 23 July and lasting upto 28 July is primarily due to a Mars directed CME, which was observed by both STEREO-A and MAVEN. Figure 6a shows the IMF and solar wind velocity observed by STEREO-A during 12 to 31 July 2017. The peak total magnetic field was 58 nT (on 24 July) and peak solar wind speed was 818 km sec^{-1} (on 25 July). Figure 6b shows the SEP intensity–time profiles of energetic protons of energy between 100 keV and 100 MeV in different channels. The maximum enhancement seen in the lowest energy channel (100 keV to 190 keV) was $>10^7$ pfu MeV^{-1} on 24 July. The different energy channels shown in Figure 6b are from SEPT ($\sim$100 keV to 2.2 MeV), LET (4 to 12 MeV), and HET (>13 to 100 MeV) particle detectors onboard STEREO-A. A dip in intensity profile is observed in all these energies on 25 July.

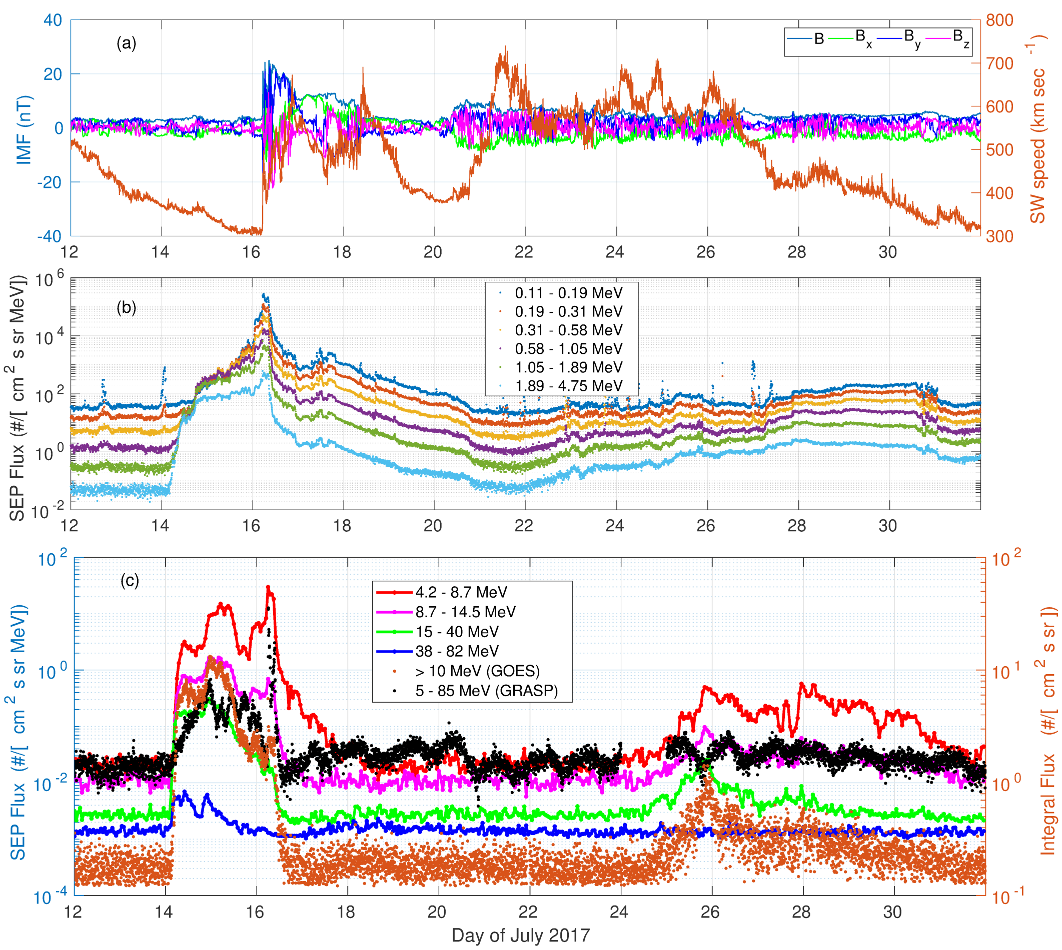

Figure 5. (a) The near Earth observations of IMF ($|B|$, B_x, B_y, B_z) and solar wind speed during 12–31 July 2017, (b) ACE observations of SEP proton intensity–time profiles during 12–31 July 2017, and (c) GOES and GRASP observations of SEP proton intensity–time profiles (GOES: differential fluxes and >10 MeV integral flux, GRASP: 5–85 MeV integral flux) during 12–31 July 2017.

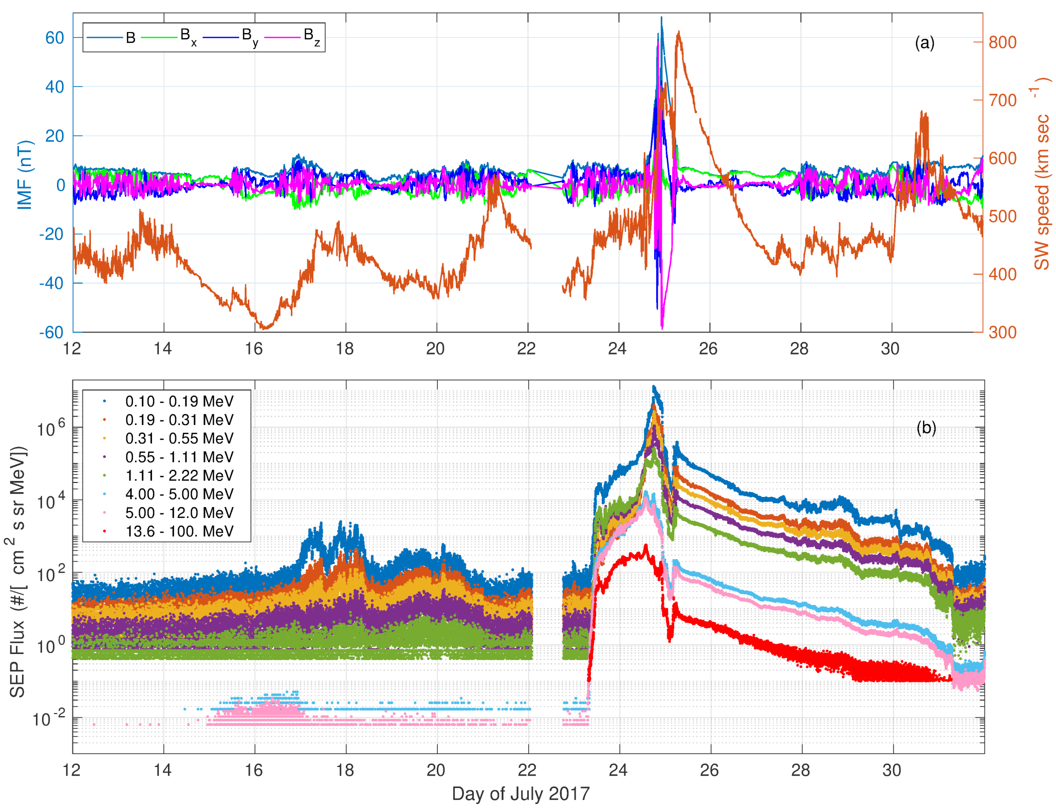

Figure 6. (a) The STEREO-A observations of IMF ($|B|$, B_x, B_y, B_z) and solar wind speed during 12–31 July 2017 and (b) STEREO-A (SEPT, LET, HET telescopes) observations of SEP proton intensity–time profiles during 12–31 July 2017. The white gap on 22 July is due to absence of data.

The CME2 event was also observed by MAVEN in orbit around Mars. Figure 7a shows the upstream solar wind velocity and magnetic field measurements from MAVEN spacecraft. Figure 7b shows the energy–time spectrogram of differential energy flux of protons from 12 to 31 July observed by the forward facing sensor one (1F) of SEP instrument onboard MAVEN. An enhancement in SEP proton flux is observed between 23 and 28 July 2017. Figure 7c shows the intensity–time profiles of protons in different energy channels between 100 keV and 5.11 MeV by forward looking sensor (1F) and Figure 7d shows the observations by reverse looking sensor (1R). A peak flux of 2×10^5 pfu MeV^{-1} was observed on 26 July in the 100 keV to 200 keV energy channel. The data just prior to the peak of proton flux enhancement are removed because of electron contamination to the proton channels, in the vicinity of peak electron flux (Luhmann et al., 2018). The reverse facing data are also shown, because the pick-up oxygen ions predominantly appear in the forward facing MAVEN/SEP detectors and hardly appear in the reverse facing detectors, and therefore confirms the presence of SEP related enhancements (Larson et al., 2015).

Two SIR events are also identified from the solar wind and magnetic field data and STEREO IMPACT Level 3 SIR events list (`https://stereo-ssc.nascom.nasa.gov/data/ins_data/impact/level3/STEREO_Level3_SIR.pdf`). One from 16 to 18 July (with a maximum solar wind speed of 493 km sec^{-1} and magnetic field intensity of 12.5 nT) and another one from 19 to 21 July (with a maximum solar wind speed of 572 km sec^{-1} and magnetic field intensity of 10.2 nT). As mentioned earlier, the former (16 July SIR) had a shock associated it (Figure 4b) with higher SEP proton intensities (Figure 6b).

Interestingly, energetic proton enhancement is also observed (at Earth) when the CME2 was not directly passing the observer, and when the observer is on the opposite side of the Sun as viewed from the CME2 longitude. Energetic proton enhancements can be seen in ACE profiles (28-30 July, Figure 5b), as well as in GOES lower energy channels such as 4.2 to 8.7 MeV (Figure 5c). This is during the period when the CME2 energetic proton event impacted STEREO-A and MAVEN, those two spacecraft were located in western heliospheric longitudes. This SEP proton enhancement observed at Earth's location is due to magnetic connections to distant shocks, that is shocks beyond heliocentric radius of the observer (Figure 5a of Luhmann et al. (2018)). The SEPMOD calculations based on the ENLIL simulation results for similar proton energy range are capturing the smaller enhancements during 28-30 July (Luhmann et al., 2018). We can also see that bulk solar wind speed and IMF do not show any significant enhancement during 27 to 31 July when the SEP proton enhancement is observed at the ACE location. However the solar wind speed is relatively higher for a period prior to the SEP proton enhancement from 21 to 26 July (Figure 5a), this could be due to the passage of a high speed stream during this period as observed from the ENLIL simulation shown in Figure 3b.

Figure 8a shows the power-law fits for SEP proton energy spectra during July 2017 events observed by ACE. The energy spectra are fitted with a power-law of the form $AE^{-\gamma}$. Two distinct SEP proton enhancements were detected by ACE from 14 to 20 July, associated with the CME1 eruption. The event averaged spectrum of the two SEP events are shown in red (14/07, 18:14 UT to 17/07, 00:43 UT) and brown (17/07, 15:50 UT to 20/07, 18:57 UT) colors. The event averaged spectrum of the SEP proton enhancement due to shock connectivity is shown in magenta color (27/07, 21:22 UT to 30/07, 15:50 UT).

Figure 8b shows the STEREO-A and MAVEN observed event averaged energy spectra during the SEP proton events of July 2017. There were two distinct SEP proton enhancements from 23 to 27 July, associated with the CME2 eruption. The spectra of these individual SEP events are shown in red (23/07, 10:48 UT to 25/07, 03:07 UT) and brown (25/07, 05:31 UT to 27/07, 23:16 UT) colors. The energy spectra are fitted with a double power law (with indices denoted as γ_a and γ_b) characterized by a spectral break at few tens of MeV. The spectral transition (or break) is observed between 6 and 10 MeV energy. A double power law or a power law with exponential rollover at a few to tens of MeV has been reported in many events (e.g. Zhao, Zhang, and Rassoul (2016)). The event averaged

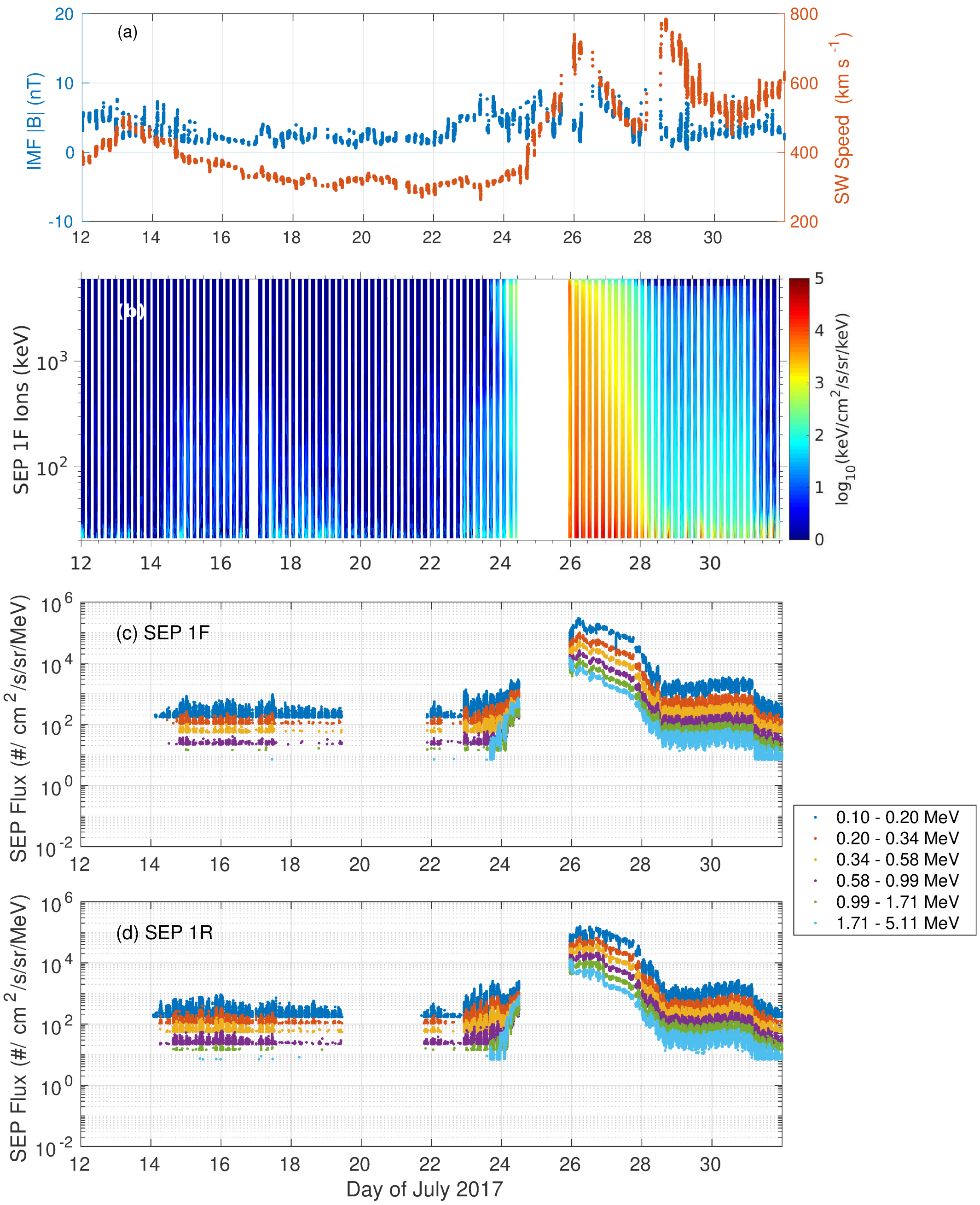

Figure 7. (a) MAVEN (near Mars) upstream observations of the IMF ($|B|$) and solar wind speed during 12–31 July 2017, (b) MAVEN observations of the SEP proton energy–time spectrogram of differential energy flux during 12–31 July 2017, (c) MAVEN observations of the SEP proton intensity–time profiles in the forward facing FOV of SEP 1 sensor during 12–31 July 2017, and (d) MAVEN observations of the SEP proton intensity–time profiles in the reverse facing FOV of SEP 1 sensor during 12–31 July 2017. The white gap before 22 July is due to low flux of particles, while after 22 July is due to poor quality of data.

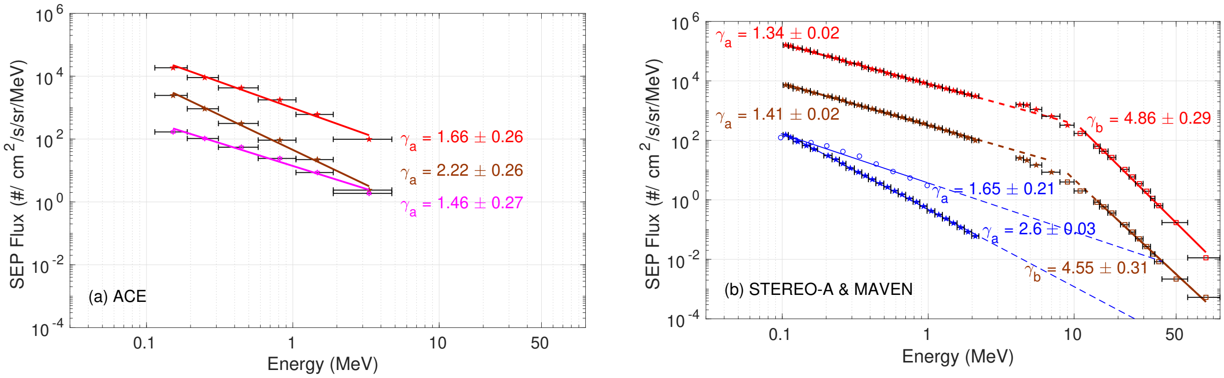

Figure 8. Power-law fits for (a) ACE, (b) STEREO-A and MAVEN observations of SEP proton events during July 2017. The left panel shows ACE observations during SEP periods from 14 to 17 July (red), 17 to 20 July (brown). The shock connected event from 27 to 30 July (magenta) is also shown. The right panel shows STEREO-A observations during SEP periods from 23 to 25 July (red), 25 to 27 July (brown). The SEP proton enhancements due to SIR event at STEREO-A (blue stars, 17 to 18 July) and MAVEN (blue circles, 14 to 17 July) are also shown - extrapolated to higher energies. The spectral indices and the uncertainties of the spectral index estimate are also indicated.

energy spectra of the CME event observed by MAVEN is not shown here due to the electron contamination to the proton channels.

The blue color fits shows the event averaged energy spectra for the SIR event observed by STEREO-A at ∼0.96 AU (17/07, 00:00 UT to 18/07, 09:50 UT) and MAVEN at ∼1.58 AU (14/07, 18:00 UT to 17/07, 13:12 UT). As mentioned earlier, the longitudinal separation between MAVEN and STEREO-A was about 46°, with the stream arriving at MAVEN before STEREO-A. The energy spectrum observed by MAVEN as well as that observed by STEREO-A are single power laws (with an index denoted as γ_a) in the energy range upto ∼2 MeV for STEREO-A, and upto ∼1 MeV for MAVEN. These are the energy ranges where we have observed particle fluxes above the background levels, at both these locations. The spectra are extrapolated to higher energies (∼40 MeV) in order to asses the differences in high energy fluxes at these two locations. We can see that the high energy proton flux is higher at Mars in comparison to the flux at 1 AU (Figure 8b).

The spectral analysis shows that the STEREO-A and Mars directed SEP events associated with the interplanetary CME2 are stronger (spectral indices of 1.3 and 1.4) than the Earth directed SEP events associated with the interplanetary CME1 (indices of 1.6 and 2.2). Also, the peak intensities are higher by around an order of magnitude for the CME2 event. The SEP event due to shock connectivity observed at Earth between 28 and 30 July is having a spectral index of 1.4 which is similar to the index of the 25 to 27 July event directly seen by STEREO-A. An onset delay of ∼2 days is observed for the shock connected event, which is due to the separation between the CME2 shock and the observer location at L1/Earth.

The 16 July SIR event observed at MAVEN and STEREO-A is having spectral indices of 1.6 and 2.6 respectively. Enhanced particle intensities by a factor of 6 (for 1 MeV protons) are observed at Mars, also the event spectrum is harder, indicating acceleration of energetic protons during the radial propagation of ∼0.62 AU. The energy spectra are extrapolated to higher energies, which shows higher proton fluxes at higher energies at Mars in comparison to 1 AU. This is important in the context of space weather, since energies of several MeV are required to degrade solar arrays, whilst energies above 40 MeV are required to disrupt electronic systems within a spacecraft.

4 Discussion

The onset time of the CME event at a location can be calculated using Velocity Dispersion Analysis (VDA), which is based on the assumptions that the first particles observed at a given distance from the Sun have been released simultaneously, propagate the same path length, and experience no scattering or energy changes (Laitinen, Huttunen-Heikinmaa, Valtonen, & Dalla, 2015). According to this, the CME event onset time,

$$t_{onset}(v) = t_{injection} + (s/v) \ ,$$

where $t_{injection}$ is the particles' injection time at the source, s is the traveled distance, and v is the particle velocity. The injection of particles starts during the CME eruption from the Sun. For the CME1 event (Earth directed), eruption starts at ∼01:25 UT on 14 July (Figure 2a, `https://cdaw.gsfc.nasa.gov/CME_list/`), the particles with a speed of 664 km sec^{-1} will arrive at 0.99 AU [ACE location] in ∼62 hours. For the CME2 event (STEREO-A and Mars directed), the eruption starts at ∼04:54 UT on 23 July (Figure 2b, `http://spaceweather.gmu.edu/seeds/secchi.php`), the CME with a speed of 811 km sec^{-1} will arrive at 0.96 AU [STEREO-A location] in ∼49 hours, while the CME will arrive at 1.58 AU [MAVEN location] in ∼81 hours. These calculations of event arrival times are matching with the observations of CME arrival at ACE (Figure 5), STEREO-A and Mars (Figures 6 and 7).

The context and space weather impacts of September 2017 solar events are extensively studied for Earth as well as for Mars (Chertok, Belov, & Abunin, 2018; Jiggens et al., 2019; Lee et al., 2018; Liu, Zhu, & Zhao, 2019; Perez-Peraza, Mrquez-Adame, Caballero-Lopez, & Manzano Islas, 2020). The active region responsible for the major flares and CMEs of September 2017 was AR 12673 (located at S09W91), while that of July 2017 was AR 12665 (located at S07W44). A southern high-latitude coronal hole was responsible for the high speed streams of July, while a southern mid-latitude coronal hole was responsible for the high speed streams of September. The events in July and September have comparable peak particle fluxes (Bruno et al., 2019; Luhmann et al., 2018). The ICME/SIR-driven interplanetary shocks of September had unusually high magnetosonic Mach numbers (Hajra, Tsurutani, & Lakhina, 2020). The angle of propagation (θ_{Bn}) of the September ICME-driven FSs varied from ∼19° to ∼90° relative to the ambient IMF directions, while their strengths varied from Mach ∼4.0 to ∼6.7 (Hajra et al., 2020). The STEREO-A observed ICME-driven FSs of July had a Mach number from ∼2.0 to ∼2.4. The θ_{Bn} of the September SIR-driven FSs varied from ∼9° to ∼84° relative to the ambient IMF directions, while their strengths varied from Mach ∼1.7 to ∼4.3 (Hajra et al., 2020). The STEREO-A observed SIR-driven FS of July had a Mach number ∼1.42 (`https://stereo-ssc.nascom.nasa.gov/data/ins_data/impact/level3/`).

Both July and September solar and SEP events had similar characteristics due to similar source region and eruptions (Luhmann et al., 2018). The spectral indices of the 4, 6, and 10 September SEP proton events are 0.5, 1.3, and 1.2 respectively for ACE observations (Bruno et al., 2019). While the spectral indices of 14 to 20 July events are 1.6 and 2.2 (Figure 8a). The spectral indices of the 4, 10, and 17 September SEP proton events are 0.2, 1.2, and 1.2 respectively for STEREO-A observations (Bruno et al., 2019). While the spectral indices of 23 to 27 July events are 1.3 and 1.4 (Figure 8b). Thus the Earth directed events of July was softer compared to the Earth directed events of September, while the STEREO-A directed events of July and September are of similar spectral characteristics. Three successive CMEs that erupted from AR 12673 during early September 2017 resulted in an intense two-step geomagnetic storm (main dip Dst$_{min}$ of -142 nT and a secondary dip

Dst$_{min}$ of -124 nT) driven by the interplanetary CME–CME interactions occurring among the eruptions involved (Scolini et al., 2020). The 16 July CME1 event caused a geomagnetic storm with Dst$_{min}$ of -72 nT, which is a smaller storm compared to the two events of September.

As mentioned earlier, for the SIR event observations at STEREO-A and Mars, enhanced proton intensities are observed by MAVEN. The spectral index observed by MAVEN is ∼1.6, which is lower than the spectral index observed by STEREO-A, which is ∼2.6 (Figure 8b). Thus the event averaged spectrum is more harder at Mars, indicating acceleration of energetic protons during the radial propagation of ∼0.62 AU. One possibility for the observed hardened spectra is that the Parker spiral is more tightly wound at larger heliocentric distances, this would make the SIR shock more quasiperpendicular (Pesses et al., 1984). These spectral index estimates of SIR-accelerated SEP enhancements are in agreement with the previous study by M. I. Desai et al. (1999), where they have shown the energy spectra of 50 keV to 20 MeV protons accelerated at SIRs at Ulysses spacecraft. If we consider the general Fisk and Lee (1980) model, it can be seen that the distribution function rolls over above ∼1 MeV energy. However, we do not see this rollover. As mentioned earlier, we do not have data points beyond ∼2 MeV (near 1 AU) and ∼1 MeV near (1.5 AU) to determine the exact rollover energy. Similar to this, proton flux enhancements near 1.5 AU associated with SIR event of June 2015 is previously reported by Thampi, Krishnaprasad, Shreedevi, Pant, and Bhardwaj (2019). The observations of SEP proton events during CMEs suggests that shock acceleration takes place within 1 AU itself during CME events (Thampi et al., 2019). The observations of SIR related SEP proton enhancements observed near Mars compared to 1 AU are important in this context because of the addition of a vantage point at 1.5 AU, and as such observations were previously sparse between 1 and 3 AU.

Helios 1 and 2 spacecraft has a long term observation of SIRs in the inner heliosphere between ∼0.3 AU and 1 AU. There are extensive observations of heliospheric conditions at 1 AU since the arrival of solar monitors at L1 point. The first detailed observations of SIRs beyond the orbit of Earth were made by the Pioneer 10 and 11 spacecraft, and the three dimensional aspect (that is, beyond the ecliptic plane) was given by Ulysses spacecraft (Balogh et al., 1999). SIR boundaries tend to steepen to form a fast forward shock at the leading edge of the interaction region and a sunward propagating reverse shock at the trailing edge of the interaction region (Richardson, 2018). Pioneer 10 and 11 observations suggests that such shocks form beyond 2 AU distances (Gosling, Hundhausen, & Bame, 1976; Hundhausen & Gosling, 1976; Smith & Wolfe, 1976). The present study suggests that strong SIR-forward shock can form even at distances like ∼1.5 AU. This could be due to the the steeping of the leading edge of the interaction region at farther distances (Hundhausen & Gosling, 1976). Also, as the stream expands at larger distances, the peak speeds are reduced and the stream would become less structured as compared to 1 AU. Intensity variation of 0.9–2.2 MeV protons measured by the Helios, Pioneer 10/11 and near-Earth spacecraft in several corotating particle events were obtained by Van Hollebeke, McDonald, Trainor, and Rosenvinge (1978), which shows that the peak intensities in corotating particle events occur at a few AU. The observations from ∼1.5 AU by MAVEN suggests that enhancement in particle intensities can happen even from 1.5 AU.

SEPs are one of the main sources of particle radiation seen in space (Jiggens et al., 2019), thus posing a major radiation risk for spacecraft systems and to astronauts in space. The transport of energetic protons through magnetically connected "roads" to diverse locations in space thus cause unexpected radiation exposure to humans in the interplanetary space, which is especially important in the context of human spaceflight. The lower spectral index measured by MAVEN during the SIR event at Mars suggests that SIR-generated protons may have harder spectra at Mars than at Earth. This is an important point for anyone assessing the radiation risk for future human exploration of Mars. It raises the question of whether there are features in space radiation environment that are more dangerous at Mars than at Earth, i.e. features where the fluxes of higher energy protons (many MeV) are greater at Mars. The results from the present study suggest that this may be the case for SIR-generated protons.

5 Summary

The solar events of July 2017 are studied using observations from multiple spacecraft near Earth, near Mars, and STEREO-A. The three heliolongitude observations, along with the radial gradient between Earth and Mars provides an opportunity to study both longitudinal and radial variation of SEPs propagating in the inner heliosphere. The STEREO-A was $\sim$125° separated from Earth, while Mars had an angular separation of $\sim$175° with respect to Earth. The widespread observations of energetic protons was associated with activity originated at NOAA AR 12665 located at the source coordinate S07W44 on the Sun.

There were two major interplanetary CME events and a SIR event during July 2017. These solar activities are particularly interesting because they have occurred during the late decay phase of the solar cycle 24. The 16 July CME1 was directed west of Earth and the 24 July CME2 was in the general direction of STEREO-A and Mars. Earth and Mars were on the opposite sides of the solar disk, while Mars and STEREO-A were aligned with respect to the nominal Parker field. The CME2 event had higher plasma velocities and around an order of magnitude higher SEP proton flux compared to the 16 July event, also the event was wider (>120°) in heliolongitude. The CME2 shock had magnetic connectivity to Earth's location, which produced an SEP proton event at L1/Earth from 28 to 30 July (Luhmann et al., 2018). An onset delay of $\sim$2 days is observed for the event arrival at ACE location. The spectral indices of the SEP proton event observed directly at STEREO-A and at the remote location of ACE was found to be similar ($\sim$1.4). The 16 July SIR event was observed by both MAVEN and STEREO-A. Higher particle intensities by a factor of 6 for 1 MeV protons, and spectral hardening from 2.6 to 1.6 are observed at 1.58 AU, indicating an acceleration of energetic protons in SIR forward shock during the radial propagation of 0.62 AU in the interplanetary space. The observations of hardened spectra at 1.58 AU compared to 0.96 AU could be due to the fact that Parker spiral is more tightly wound at larger heliocentric distances, making the SIR shock more quasi-perpendicular.

Thus, the following major inferences are drawn from the study,

a) An energetic proton enhancement event was observed at 1 AU due to magnetic connectivity with a distant CME-driven shock, and the spectral index was found to be invariant with the source location. That is, the power-law spectral index of the SEP proton energy spectra remained the same at the source location as well as at a location which is magnetically connected.

b) The SIR forward shock of 16 July 2017 found to accelerate energetic protons between 0.96 AU and 1.58 AU. The comparison of energy spectra at these two vantage points shows that the spectra hardens as the energetic protons accelerates. One possibility is that the Parker spiral is more tightly wound at larger heliocentric distances. This would make the shock more steep. This is an important aspect considering the radiation risk during the human exploration to Mars.

Acknowledgments

The work is supported by the Indian Space Research Organisation (ISRO). The MAVEN data used in this work are taken from the Planetary Data System (`https://pds.nasa.gov/`). We gratefully acknowledge the MAVEN team for the data. The ACE EPAM/SWEPAM/MAG data are taken from the ACE Science Center (`http://www.srl.caltech.edu/ACE/ASC/`). The STEREO-A IMPACT/PLASTIC data are taken from STEREO Science Center at `http://www.srl.caltech.edu/STEREO/`. The SDO AIA images are from `https://sdo.gsfc.nasa.gov/`. The STEREO-A/SECCHI EUVI and COR2 images are from STEREO Science Center at `https://stereo-ssc.nascom.nasa.gov/`. The SOHO LASCO images are from `https://soho.nascom.nasa.gov/`. The GOES SEP flux data are obtained from the SPDF OMNIWeb data center (`https://omniweb.gsfc.nasa.gov/`). We thank the staff of the ACE and STEREO Science Centers for providing the ACE and STEREO data and OMNIWeb team for providing the GOES data. The WSA-ENLIL+Cone model simulations are provided by CCMC through their public Runs on Request system (`https://ccmc.gsfc.nasa.gov/`; run number: Leila_Mays_080917_SH_1). We thank M. L. Mays, CCMC, NASA GSFC for their openly available simulation runs. C. Krishnaprasad acknowledges the financial assistance provided by ISRO through a research fellowship. This research has made use of SunPy v1.1, an open-source and free community-developed solar data analysis Python package (`https://sunpy.org/`).

References

Balogh, A., Gosling, J. T., Jokipii, J. R., Kallenbach, R., & Kunow, H. (Eds.). (1999). *Corotating interaction regions*. Springer Netherlands. doi: 10.1007/978-94-017-1179-1

Blake, J. B., Fennell, J. F., Turner, D. L., Cohen, I. J., & Mauk, B. H. (2019). Delayed arrival of energetic solar particles at MMS on 16 July 2017. *Journal of Geophysical Research: Space Physics*, *124*(4), 2711-2719. doi: 10.1029/2018JA026341

Bruno, A., Christian, E. R., de Nolfo, G. A., Richardson, I. G., & Ryan, J. M. (2019). Spectral analysis of the September 2017 solar energetic particle events. *Space Weather*, *17*(3), 419-437. doi: 10.1029/2018SW002085

Cane, H. V., Reames, D. V., & von Rosenvinge, T. T. (1988). The role of interplanetary shocks in the longitude distribution of solar energetic particles. *J. Geophys. Res*, *93*(A9), 9555-9567. doi: 10.1029/JA093iA09p09555

Chertok, I. M., Belov, A. V., & Abunin, A. A. (2018). Solar eruptions, Forbush decreases, and geomagnetic disturbances from outstanding active region 12673. *Space Weather*, *16*(10), 1549-1560. doi: 10.1029/2018SW001899

Chollet, E. E., Mewaldt, R. A., Cummings, A. C., Gosling, J. T., Haggerty, D. K., Hu, Q., ... Sauvaud, J.-A. (2010). Multipoint connectivity analysis of the May 2007 solar energetic particle events. *Journal of Geophysical Research: Space Physics*, *115*(A12). doi: 10.1029/2010JA015552

da Costa Jr., E., Tsurutani, B. T., Alves, M. V., Echer, E., & Lakhina, G. S. (2013). Cross-field diffusion of 100 keV to 2 MeV protons in interplanetary space. *The Astrophysical Journal*, *778*(2), 180. doi: 10.1088/0004-637x/778/2/180

Desai, M., & Giacalone, J. (2016). Large gradual solar energetic particle events. *Living Reviews in Solar Physics*, *13*(1), 3. doi: 10.1007/s41116-016-0002-5

Desai, M. I., Marsden, R. G., Sanderson, T. R., Lario, D., Roelof, E. C., Simnett, G. M., ... Forsyth, R. J. (1999). Energy spectra of 50-keV to 20-MeV protons accelerated at corotating interaction regions at Ulysses. *Journal of Geophysical Research: Space Physics*, *104*(A4), 6705-6719. doi: 10.1029/1998JA900176

Dumbović, M., Guo, J., Temmer, M., Mays, M. L., Veronig, A., Heinemann, S. G., ... Wimmer–Schweingruber, R. F. (2019). Unusual plasma and particle signatures at Mars and STEREO-A related to CME–CME interaction. *The Astrophysical Journal*, *880*(1), 18. doi: 10.3847/1538-4357/ab27ca

Fisk, L. A., & Lee, M. A. (1980). Shock acceleration of energetic particles in corotating interaction regions in the solar wind. *The Astrophysical Journal*, *237*, 620-626. doi: 10.1086/157907

Gold, R., Krimigis, S., Hawkins, S., Haggerty, D., Lohr, D., Fiore, E., ... Lanzerotti, L. (1998). Electron, Proton, and Alpha Monitor on the Advanced Composition Explorer spacecraft. *Space Science Reviews*, *86*(1), 541–562. doi: 10.1023/A:1005088115759

Gosling, J. T., Hundhausen, A. J., & Bame, S. J. (1976). Solar wind stream evolution at large heliocentric distances: Experimental demonstration and the test of a model. *Journal of Geophysical Research*, *81*(13), 2111-2122. doi: 10.1029/JA081i013p02111

Hajra, R., Tsurutani, B. T., & Lakhina, G. S. (2020). The complex space weather events of 2017 September. *The Astrophysical Journal*, *899*(1), 3. doi: 10.3847/1538-4357/aba2c5

Halekas, J. S., Ruhunusiri, S., Harada, Y., Collinson, G., Mitchell, D. L., Mazelle, C., ... Jakosky, B. M. (2017). Structure, dynamics, and seasonal variability of the Mars-solar wind interaction: MAVEN Solar Wind Ion Analyzer in-flight performance and science results. *Journal of Geophysical Research: Space Physics*, *122*(1), 547-578. doi: 10.1002/2016JA023167

Hundhausen, A. J., & Gosling, J. T. (1976). Solar wind structure at large heliocentric distances: An interpretation of pioneer 10 observations. *Journal of Geophysical Research*, *81*(7), 1436–1440. doi: 10.1029/ja081i007p01436

Jian, L. K., Russell, C. T., Luhmann, J. G., Galvin, A. B., Simunac, K. D. C., Zank, G. P., ... Verkhoglyadova, O. (2013). Solar wind observations at STEREO: 2007 - 2011. *AIP Conference Proceedings*, *1539*(1), 191-194. doi: 10.1063/1.4811020

Jiggens, P., Clavie, C., Evans, H., O'Brien, T. P., Witasse, O., Mishev, A. L., ... Nagatsuma, T. (2019). In situ data and effect correlation during September 2017 solar particle event. *Space Weather*, *17*(1), 99-117. doi: 10.1029/2018SW001936

Klein, K.-L., & Dalla, S. (2017). Acceleration and propagation of solar energetic particles. *Space Science Reviews*, *212*(3), 1107–1136. doi: 10.1007/s11214-017-0382-4

Krishnaprasad, C., Thampi, S. V., & Bhardwaj, A. (2019). On the response of Martian ionosphere to the passage of a corotating interaction region: MAVEN observations. *Journal of Geophysical Research: Space Physics*, *124*(8), 6998-7012. doi: 10.1029/2019JA026750

Laitinen, T., Huttunen-Heikinmaa, K., Valtonen, E., & Dalla, S. (2015). Correcting for interplanetary scattering in velocity dispersion analysis of solar energetic particles. *The Astrophysical Journal*, *806*(1), 114. doi: 10.1088/0004-637x/806/1/114

Larson, D. E., Lillis, R. J., Lee, C. O., Dunn, P. A., Hatch, K., Robinson, M., ... Jakosky, B. M. (2015). The MAVEN Solar Energetic Particle investigation. *Space Science Reviews*, *195*(1), 153–172. doi: 10.1007/s11214-015-0218-z

Lee, C. O., Jakosky, B. M., Luhmann, J. G., Brain, D. A., Mays, M. L., Hassler, D. M., ... Halekas, J. S. (2018). Observations and impacts of the 10 September 2017 solar events at Mars: An overview and synthesis of the initial results. *Geophysical Research Letters*, *45*(17), 8871-8885. doi: 10.1029/2018GL079162

Liu, Y. D., Zhao, X., Hu, H., Vourlidas, A., & Zhu, B. (2019). A comparative study of 2017 July and 2012 July complex eruptions: Are solar superstorms "perfect storms" in nature? *The Astrophysical Journal Supplement Series*, *241*(2), 15. doi: 10.3847/1538-4365/ab0649

Liu, Y. D., Zhu, B., & Zhao, X. (2019). Geometry, kinematics, and heliospheric impact of a large CME-driven shock in 2017 September. *The Astrophysical Journal*, *871*(1), 8. doi: 10.3847/1538-4357/aaf425

Luhmann, J. G., Mays, M. L., Li, Y., Lee, C. O., Bain, H., Odstrcil, D., ... Petrie, G. (2018). Shock connectivity and the late cycle 24 solar energetic particle events in July and September 2017. *Space Weather*, *16*(5), 557-568. doi: 10.1029/2018SW001860

Mays, M. L., Taktakishvili, A., Pulkkinen, A., MacNeice, P. J., Rastätter, L., Odstrcil, D., ... Kuznetsova, M. M. (2015). Ensemble modeling of CMEs using the WSA–ENLIL+Cone model. *Solar Physics*, *290*(6), 1775–1814. doi: 10.1007/s11207-015-0692-1

Mewaldt, R. A., Cohen, C. M. S., Cook, W. R., Cummings, A. C., Davis, A. J., Geier, S., ... Wortman, K. (2008). The Low-Energy Telescope (LET) and SEP Central Electronics for the STEREO Mission. *Space Science Reviews*, *136*(1), 285–362. doi: 10.1007/s11214-007-9288-x

Müller-Mellin, R., Böttcher, S., Falenski, J., Rode, E., Duvet, L., Sanderson, T., ... Smit, H. (2008). The Solar Electron and Proton Telescope for the STEREO Mission. *Space Science Reviews*, *136*(1), 363–389. doi: 10.1007/s11214-007-9204-4

Odstrcil, D. (2003). Modeling 3-D solar wind structure. *Advances in Space Research*, *32*(4), 497 - 506. (Heliosphere at Solar Maximum) doi: 10.1016/S0273-1177(03)00332-6

Paouris, E., & Mavromichalaki, H. (2017). Effective Acceleration Model for the Arrival Time of Interplanetary Shocks driven by Coronal Mass Ejections. *Solar Physics*, *292*(12), 180. doi: 10.1007/s11207-017-1212-2

Parker, E. N. (1958). Dynamics of the Interplanetary Gas and Magnetic Fields. *The Astrophysical Journal*, *128*, 664. doi: 10.1086/146579

Patel, M., Li, Z., Hudson, M., Claudepierre, S., & Wygant, J. (2019). Simulation of prompt acceleration of radiation belt electrons during the 16 July 2017 storm. *Geophysical Research Letters*, *46*(13), 7222-7229. doi: 10.1029/2019GL083257

Perez-Peraza, J. A., Mrquez-Adame, J. C., Caballero-Lopez, R. A., & Manzano Islas, R. R. (2020). Spectra of the two official GLEs of solar cycle 24. *Advances in Space Research*, *65*(1), 663 - 676. doi: 10.1016/j.asr.2019.10.021

Pesses, M. E., Van Allen, J. A., Tsurutani, B. T., & Smith, E. J. (1984). High time resolution observations of corotating interaction region proton events by Pioneer 11. *Journal of Geophysical Research: Space Physics*, *89*(A1), 37-46. doi: 10.1029/JA089iA01p00037

Rahmati, A., Larson, D. E., Cravens, T. E., Lillis, R. J., Dunn, P. A., Halekas, J. S., ... Jakosky, B. M. (2015). MAVEN insights into oxygen pickup ions at Mars. *Geophysical Research Letters*, *42*(21), 8870-8876. doi: 10.1002/2015GL065262

Reames, D. V. (1995). Solar energetic particles: A paradigm shift. *Reviews of Geophysics*, *33*(S1), 585–589. doi: 10.1029/95RG00188

Reames, D. V. (2013). The two sources of solar energetic particles. *Space Science Reviews*, *175*(1), 53–92. doi: 10.1007/s11214-013-9958-9

Richardson, I. G. (2018). Solar wind stream interaction regions throughout the heliosphere. *Living Reviews in Solar Physics*, *15*(1). doi: 10.1007/s41116-017-0011-z

Richardson, I. G., von Rosenvinge, T. T., Cane, H. V., Christian, E. R., Cohen, C. M. S., Labrador, A. W., ... Stone, E. C. (2014). >25 MeV Proton Events Observed by the High Energy Telescopes on the STEREO A and B Spacecraft and/or at Earth During the First Seven Years of the STEREO Mission. *Solar Physics*, *289*(8), 3059–3107. doi: 10.1007/s11207-014-0524-8

Scolini, C., Chané, E., Temmer, M., Kilpua, E. K. J., Dissauer, K., Veronig, A. M., ... Poedts, S. (2020). CME–CME interactions as sources of CME geoeffectiveness: The formation of the complex ejecta and intense geomagnetic storm in 2017 early September. *The Astrophysical Journal Supplement Series*, *247*(1), 21. doi: 10.3847/1538-4365/ab6216

Smith, E. J., & Wolfe, J. H. (1976). Observations of interaction regions and corotating shocks between one and five AU: Pioneers 10 and 11. *Geophysical Research Letters*, *3*(3), 137-140. doi: 10.1029/GL003i003p00137

Thampi, S. V., Krishnaprasad, C., Bhardwaj, A., Lee, Y., Choudhary, R. K., & Pant, T. K. (2018). MAVEN observations of the response of Martian ionosphere to the interplanetary coronal mass ejections of March 2015. *Journal of Geophysical Research: Space Physics*, *123*(8), 6917 - 6929. doi: 10.1029/2018JA025444

Thampi, S. V., Krishnaprasad, C., Shreedevi, P. R., Pant, T. K., & Bhardwaj, A. (2019). Acceleration of energetic ions in corotating interaction region near 1.5 AU: Evidence from MAVEN. *The Astrophysical Journal Letters*, *880*(1), L3. doi: 10.3847/2041-8213/ab2b43

Tsurutani, B., Gonzalez, W., Zhou, X.-Y., Lepping, R., & Bothmer, V. (2004). Properties of slow magnetic clouds. *Journal of Atmospheric and Solar-Terrestrial Physics*, *66*(2), 147 - 151. (Space Weather in the Declining Phase of the Solar Cycle) doi: 10.1016/j.jastp.2003.09.007

Tsurutani, B., Lakhina, G., Verkhoglyadova, O., Gonzalez, W., Echer, E., & Guarnieri, F. (2011). A review of interplanetary discontinuities and their geomagnetic effects. *Journal of Atmospheric and Solar-Terrestrial Physics*, *73*(1), 5 - 19. doi: 10.1016/j.jastp.2010.04.001

Tsurutani, B. T., & Lin, R. P. (1985). Acceleration of >47 keV ions and >2 keV electrons by interplanetary shocks at 1 AU. *Journal of Geophysical Research: Space Physics*, *90*(A1), 1-11. doi: 10.1029/JA090iA01p00001

Tsurutani, B. T., Smith, E. J., Pyle, K. R., & Simpson, J. A. (1982). Energetic protons accelerated at corotating shocks: Pioneer 10 and 11 observations from 1 to 6 AU. *Journal of Geophysical Research: Space Physics*, *87*(A9), 7389-7404. doi: 10.1029/JA087iA09p07389

Tsurutani, B. T., & Thorne, R. M. (1982). Diffusion processes in the magnetopause boundary layer. *Geophysical Research Letters*, *9*(11), 1247-1250. doi: 10.1029/GL009i011p01247

Tsurutani, B. T., Verkhoglyadova, O. P., Mannucci, A. J., Lakhina, G. S., Li, G., & Zank, G. P. (2009). A brief review of solar flare effects on the ionosphere. *Radio Science*, *44*(1). doi: 10.1029/2008RS004029

Tsurutani, B., Wu, S. T., Zhang, T. X., & Dryer, M. (2003). Coronal mass ejection (CME)-induced shock formation, propagation and some temporally and spatially developing shock parameters relevant to particle energization. *A&A*, *412*(1), 293-304. doi: 10.1051/0004-6361:20031413

Van Hollebeke, M. A. I., Ma Sung, L. S., & McDonald, F. B. (1975). The Variation of Solar Proton Energy Spectra and Size Distribution with Heliolongitude. *Solar Physics*, *41*(1), 189-223. doi: 10.1007/BF00152967

Van Hollebeke, M. A. I., McDonald, F. B., Trainor, J. H., & Rosenvinge, T. T. (1978). The radial variation of corotating energetic particle streams in the inner and outer solar system. *Journal of Geophysical Research: Space Physics*, *83*(A10), 4723-4731. doi: 10.1029/JA083iA10p04723

von Rosenvinge, T. T., Reames, D. V., Baker, R., Hawk, J., Nolan, J. T., Ryan, L., … Wiedenbeck, M. E. (2008). The High Energy Telescope for STEREO. *Space Science Reviews*, *136*(1), 391–435. doi: 10.1007/s11214-007-9300-5

von Rosenvinge, T. T., Richardson, I. G., Reames, D. V., Cohen, C. M. S., Cummings, A. C., Leske, R. A., … Wiedenbeck, M. E. (2009). The solar energetic particle event of 14 December 2006. *Solar Physics*, *256*(1), 443–462. doi: 10.1007/s11207-009-9353-6

Xie, H., Mkel, P., St.Cyr, O. C., & Gopalswamy, N. (2017). Comparison of the coronal mass ejection shock acceleration of three widespread SEP events during solar cycle 24. *Journal of Geophysical Research: Space Physics*, *122*(7), 7021-7041. doi: 10.1002/2017JA024218

Zhang, M., Qin, G., & Rassoul, H. (2009). Propagation of solar energetic particles in three-dimensional interplanetary magnetic fields. *The Astrophysical Journal*, *692*(1), 109–132. doi: 10.1088/0004-637x/692/1/109

Zhao, L., Zhang, M., & Rassoul, H. K. (2016). Double power laws in the event-integrated solar energetic particle spectrum. *The Astrophysical Journal*, *821*(1), 62. doi: 10.3847/0004-637X/821/1/62